Effect of cooling rate and aluminum contents on the Mg-Al-Zn alloys' structure and mechanical properties

L.A. Dobrzański*, M. Król, T. Tański

Division of Material Processing Technology, Management and Computer Techniques in Materials Science, Institute of Engineering Materials and Biomaterials, Silesian University of Technology, ul. Konarskiego 18a, 44-100 Gliwice, Poland
* Corresponding author: E-mail address: leszek.dobrzanski@polsl.pl

Methodology of research

ABSTRACT

Purpose: This work present an influence of Al concentration and cooling rate on structure and mechanical properties of magnesium alloys. Also the paper presents a methodology to predict crystallization temperatures obtained during crystallization process using an UMSA platform, based on cooling rate and chemical composition and mechanical properties and grain size based on characteristics temperatures.

Design/methodology/approach: The experimental magnesium alloy used for thermal analysis and training of neural network was prepared in cooperation with the Faculty of Metallurgy and Materials Engineering of the Technical University of Ostrava and the CKD Motory plant, Hradec Kralove in the Czech Republic. The alloy was cooled with three different cooling rates in UMSA Technology Platform. The following results concern scanning electron microscopy investigations in the SE observation mode, as well as using BSE modus for better phase contrast results, also quantitative microanalysis was applied for chemical composition investigations of the phases occurred. Compression test were conducted at room temperature using a Zwick universal testing machine. Compression specimens were tested corresponding to each of three cooling rates. Rockwell F-scale hardness tests were carried out using a Zwick HR hardness testing machine.

Findings: The research show that the thermal analysis carried out on UMSA Technology Platform is an efficient tool for collect and calculate thermal parameters. The formation temperatures of various thermal parameters, mechanical properties (hardness and ultimate compressive strength) and grain size are shifting with an increasing cooling rate.

Practical implications: The parameters described can be applied in metal casting industry for selecting magnesium ingot preheating temperature for semi solid processing to achieve requirements properties. The presented models can be applied in computer systems of Mg-Al-Zn casting alloys, selection and designing for Mg-Al-Zn casting parts.

Originality/value: The paper contributes to better understanding and recognition an influence of different solidification condition on non-equilibrium thermal parameters of magnesium alloys.

Keywords: Thermal treatment; Mechanical properties; Magnesium alloys

1. Introduction

The application of thermal analysis in different fields of science and engineering is an extensive topic which has been the subject of significant interest particularly since the beginning of the modern era of thermal analysis in the early 1960s. With the continuous development of new techniques using modern computers, more and more applications are constantly being explored and reported. In the last several years, applications on the fields of cement chemistry, clays and minerals, polymeric materials, pharmaceuticals and other general applications have been discussed in detail. Thermal analysis techniques have also been used extensively in the field of metallurgy and a large number of publications (several thousands in the last four decades). On this subject have been identified in the literature. For obvious practical reasons, however, only a select number of publications, in which thermal analyses were used as primary techniques or important supplementary techniques, were chosen to address metallurgical topics that have received most attention in the recent past. From the many thermal analysis techniques that have been used in a wide variety of applications, thermogravimetry (TG), differential thermal analysis (DTA) and differential scanning calorimetry (DSC) were found to be the most commonly used in metallurgy [1-3].

Table 1.
Thermal methods [1]

Technique	Abbreviation	Property	Uses
Thermogravimetry	TG	Mass	Decompositions
(Thermogravimetric analysis)	TGA		Oxidations
Differential thermal analysis	DTA	Temperature difference	Phase changes, reactions
Differential scanning calorimetry	DSC	Power difference of heat flow	Heat capacity, phase changes, reactions
Thermomechanical analysis	TMA	Deformations	Mechanical changes
Dynamic mechanical analysis	DMA	Dimensional change Moduli	Expansion Phase changes, glass transitions, polymer curve
Dielectric thermal analysis	DETA	Electrical	As DMA
Evolved gas analysis	EGA	Gases evolved or reacted	Decompositions
Thermiptometry		Optical	Phase changes, surface reactions, colour changes
Less frequently used methods Thermosonimetry	TS	Sound	Mechanical and chemical changes
Thermoluminescence	TL	Light emitted	Oxidation
Thermomagnetometry	TM	Magnetic	Magnetic changes

Every thermal method studies and measure a property as a function of temperature. The properties studied may include almost every physical or chemical property of the sample, or its product. The more frequently used thermal analysis techniques are shown in Table 1 together with the names most usually employed for them [1].

The modern instrumentation used for any experiment in thermal analysis or calorimetry is usually made up of four major parts [2, 4]:
- the sample and a container or holder;
- sensors to detect and measure a particular property of the sample and to measure temperature;
- an enclosure within the experimental parameters (e.g. temperature, pressure, gas atmosphere) may be controlled;
- a computer to control the experimental parameters, such as the temperature programme, to collect the data from the sensors and to process the data to produce meaningful results and records.

Sometimes in literature can be found an acronym SCRAM which mean sample-crucible-rate of heating-atmosphere-mass. It enable the analyst to obtain good, reproducible results for most thermal methods provided that the following details are recorded for each run:

The *sample*: A proper chemical description must be given together with the source and pre-treatments. The history of the sample, impurities and dilution with inert material can all affect results.

The *crucible.* The material and shape of the crucible or sample holder is important. Deep crucibles may restrict gas flow more than flat, wide ones, and platinum crucibles catalyse come reactions more than alumina ones. The type of holder or clamping used for Thermomechanical methods is equally important. The make and type of instrument used should also be recorded.

The *rate of heating:* this has most important effects. A very slow heating rate will allow the reactions to come closer to equilibrium and there will be less thermal lag in the apparatus. Conversely, high heating rate will give a faster experiment, deviate more from equilibrium and cause greater thermal lag. The parameters of special heating programmes, such as modulated temperature or sample control, must be noted.

The *atmosphere:* both the transfer of heat, the supply and removal of gaseous reactants and the nature of reactions which occur, or are prevented, depend on chemical nature of the reactions and its flow. Oxidations will occur well in oxygen, less so in air and not at all in argon. Product removal by a fairly rapid gas flow may prevent reverse reactions occurring.

The *mass of the sample:* A large mass of sample will require more energy, and heat transfer will be determined by sample mass and dimensions. These include the volume, packing, and particle size of the sample. Fine powders react rapidly, lumps more slowly. Large samples may allow the detection of small effects. Comparison of runs should preferably be made using similar sample masses, sizes and shapes.

Specific techniques require the recording of other parameters, for example the load on the sample in thermomechanical analysis. Calorimetric methods, too, require attention to the exact details of each experiment.

Thermal Analysis techniques are used in a wide range of disciplines, from pharmacy and foods to polymer science, materials and glasses; in fact any field where changes in

sample behaviour are observed under controlled heating or controlled cooling conditions. The wide range of measurements possible provide fundamental information on the material properties of the system under test, so thermal analysis has found increasing use both in basic characterisation of materials and in a wide range of applications in research, development and quality control in industry and academia [1-4].
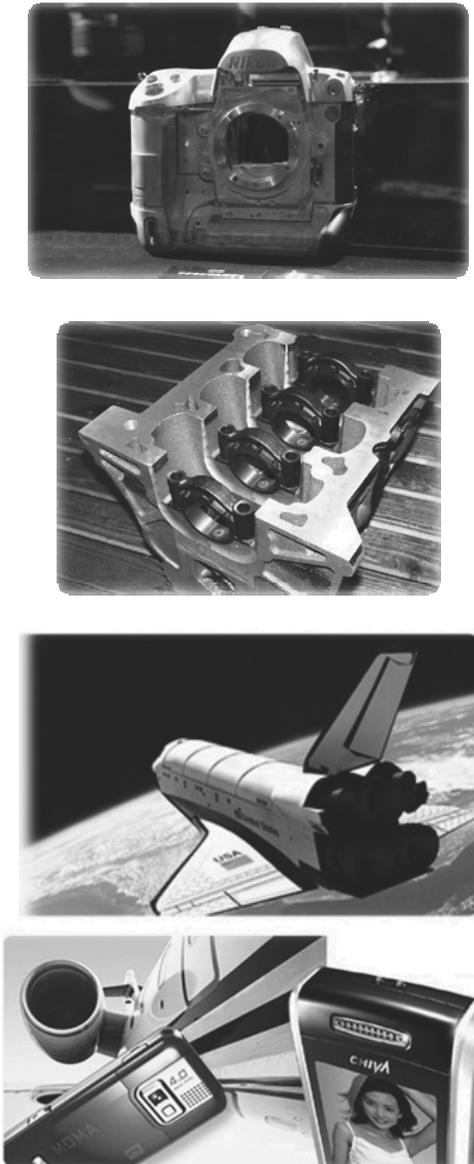
Fig. 1. Examples of application magnesium alloys

For the experimental determination of phase diagrams the use of different techniques can be beneficial. The role of thermal analysis has been of primary importance since the beginning of this research field, as has been pointed out by different authors [2, 4, 5].

Thermal analysis as a technique is used to evaluate the melt quality. By this method, some characteristic values are extracted from a cooling curve and/or its derivative, and then a regression relationship is built up between the characteristics and quality indexes as grain size, eutectic structure, silicon morphology, and so on [1].

In metal casting industry an improvement of component quality mainly depends on better control over the production parameters. Thus, computer-aided cooling curve thermal analysis of alloys is extensively used for the evaluation of several processing and material parameters. Thermal analysis of alloys can provide information about the composition of the alloy, the latent heat of solidification, the evolution of the fraction solid, the types of phases that solidify, and even dendrite coherency. There are also many other uses for thermal analysis, such as, determining dendrite arm spacing, degree of modification and grain refining in aluminium alloys, the liquidus and solidus temperature, and characteristic temperatures related to the eutectic regions and intermetallic phase formation [6, 7].

As the lightest metal construction material, magnesium is extremely attractive for many lightweight construction applications (Fig. 1). Due to the high strength of magnesium in comparison to its weight, magnesium die casting is particularly suitable for many types of equipment housings. Magnesium is attractive for more than just its weight – due to the low viscosity of the melt, highly complex components can be manufactured with thinner walls and larger surface areas than die cast aluminium. The good heat conductivity and electromagnetic screening of die cast magnesium make it attractive for many segments of machine construction and the electronics industry. The disadvantage of high corrosion from other metals or acids can be counted by high purity magnesium alloys, design measures and suitable surface protection such as passivation, anodizing or coatings [8-10].

In its pure form, magnesium is soft, mechanically weak, and hence not generally used for structural applications. By careful selection of alloying elements, alloys can be produced - both for general-purpose and for special applications. As with other metallic alloy systems, a combination of well-known hardening mechanisms (solid solution hardening, particle dispersion hardening, work hardening, and grain boundary hardening) determines the mechanical properties of magnesium alloys. Alloying additions influence other properties including reactivity of the melt, castability, and corrosion performance [9, 10].

The alloying elements used with magnesium can be grouped into two categories [11, 12]:

- elements that actively influence the melt. Examples are: beryllium (≤15ppm), which lowers the rate of melt oxidation, and manganese (<= 0.6 wt%), which reduces the iron content and hence the corrosion rate of the alloys. These additions are active in relatively small amounts and do not require extensive solubility in the melt.
- elements that modify the microstructure of the alloy via the above-mentioned hardening mechanisms. This group includes elements that influence castability. Except for grain-refining additions (carbon inoculation), which can be active in small amounts, these elements must be relatively soluble in liquid magnesium. Commercially interesting alloying elements include aluminum, cerium, copper, lanthanum, lithium, manganese, neodymium, silver, thorium, yttrium, zinc, and zirconium.

Magnesium's physical properties are certainly influenced by the amount of added constituents. The effect of the constituent added is mostly directly pro rata to its amount. The processing and property effects of the individual alloying elements are more important in most structural applications than the physical properties. Here is a description of each alloying constituent's effect on the alloy quality.

Aluminum has the most favorable effect on magnesium of any of the alloying elements. It improves strength and hardness, and it widens the freezing range, and makes the alloy easier to cast. When exceeding 6 wt%, the alloy becomes heat treatable, but commercial alloys rarely exceed 10 wt% aluminum. An aluminum content of 6 wt% yields the optimum combination of strength and ductility [13].

Zinc is next to aluminum in effectiveness, as an alloying ingredient in magnesium. It is often used in combination with aluminum to produce improvement in room-temperature strength; however, it increases hot shortness when added in amounts greater than 1 wt% to magnesium alloys containing 7-10 wt% aluminum. Zinc is also used in combination with zirconium, rare earths, or thorium to produce precipitation-hardenable magnesium alloys having good strength. Zinc also helps overcome the harmful corrosive effect of iron and nickel impurities that might be present in the magnesium alloy.

Calcium is added in very small amounts, being a special alloying component. It has a dual purpose: when added to casting alloys immediately prior to pouring, it reduces oxidation in the molten condition as well as during subsequent heat treatment of the casting, and it improves the rollability of magnesium sheet. However, the addition of calcium must be controlled so that it is below about 0.3 wt% - or the sheet will be susceptible to cracking during welding.

Manganese does not affect tensile strength considerably, yet it slightly increases the yield strength. Its most important function is to improve saltwater resistance of Mg-Al and Mg-Al-Zn alloys by removing iron and other heavy-metal elements into relatively harmless intermetallic compounds, some of which separate out during melting. The amount of manganese that can be added is limited by its relatively low solubility in magnesium. Commercial alloys containing manganese rarely contain over 1.5 wt%, and in the presence of aluminum, the solid solubility of manganese is reduced to about 0.3 wt%.

Copper adversely affects the corrosion resistance of magnesium if present in amounts exceeding 0.05 wt%. However, it improves high-temperature strength.

Iron is one of the most harmful impurities in magnesium alloys due to considerable reduction of corrosion resistance even in present in small amounts. In ordinary commercial-grade alloys, the iron content can average as high as 0.01-0.03 wt%. However, for maximum corrosion resistance, 0.005% is specified as the upper limit for iron content.

Nickel , just like iron, is another harmful impurity in magnesium alloys because it also reduces the corrosion resistance if present, even in small amounts. In ordinary commercial-grade alloys, the nickel content can average as high as 0.01-0.03 wt%, but for maximum resistance to corrosion, 0.005% is specified as the upper limit for nickel content.

Lithium has relatively high solid solubility in magnesium (5.5 wt%, 17.0 at.%) and low relative density (0.54). It has attracted interest as an alloying element in magnesium alloys to lower the density to values even lower than that of unalloyed magnesium. Moreover, only some 11 wt% of lithium is needed to form the β phase, which has a body-centered cubic crystal structure, thereby improving formability of wrought products. The addition of lithium decreases strength, but increases ductility. Mg-Li alloys are also amenable to age hardening, although they tend to overage at only slightly elevated temperatures. Nevertheless, the Mg-Li alloys have found only limited application [8-10, 25, 27].

Silicon increases fluidity of the metal in the molten state. However, it decreases corrosion resistance of magnesium alloys in case of iron presence in the alloy.

Silver additions improve the mechanical properties of magnesium alloys by increasing response to age hardening.

Thorium increases the creep strength of magnesium alloys at temperatures up to 370°C. The most common alloys contain 2-3 wt% thorium in combination with zinc, zirconium, or manganese. Thorium improves the weldability of zinc-containing alloys.

Tin is useful when alloyed with magnesium in combination with small amounts of aluminum. It increases the ductility of the alloy and makes it better for hammer forging, because it reduces the tendency for the alloy to crack while being hot-worked.

Yttrium has a relatively high solid solubility in magnesium (12.4 wt%) and is added with other rare earths to promote creep resistance at temperatures up to 300°C. About 4-5% Zr is added to magnesium to form commercial alloys such as WE54 and WE43, where it imparts good elevated-temperature properties up to about 250°C.

Zirconium has a powerful grain-refining effect on magnesium alloys. It is added to alloys containing zinc, rare earths, thorium, or a combination of these elements, where it serves as a grain refiner (up to its limit of solid solubility). However, it cannot be used in alloys containing aluminum or manganese because it forms stable compounds with these elements and is thus removed from solid solution. It also forms stable compounds with any iron, silicon, carbon, nitrogen, oxygen, and hydrogen present in the melt. Because only the portion of the zirconium content available for grain refining is that which is in solid solution, the soluble zirconium content, rather than the total zirconium content, is the value important to the alloy.

Rare earth metals are added to magnesium alloys either as mischmetal or as didymium. Mischmetal is a natural mixture of rare earths containing about 50 wt% cerium, the remainder being mainly lanthanum and neodymium; didymium is a natural mixture of approximately 85% neodymium and 15% praseodymium. Additions of rare earths increase the strength of magnesium alloys at elevated temperatures. They also reduce weld cracking and porosity in casting because they narrow the freezing range of the alloys.

A series of high-performance magnesium-based alloys was developed after discovery of the extremely efficient grain-refining action of zirconium. This effect results from the formation of high-density tiny zirconium particles in the melt, which act as potent grain nuclei.

Unfortunately, elements such as aluminum and manganese lower the solubility of zirconium in the melt, thus precluding exploitation of the grain-refining mechanism in common aluminum-containing alloys.

Mg-Zn-RE-Zr. Binary Mg-Zn alloys show inferior mechanical properties and castability, but the addition of zirconium for grain refinement and rare earth (RE) elements to reduce microporosity, led to the development of alloys such as EZ33 and ZE41. These alloys have been used widely as sand castings in the T5 condition (cooled and artificially aged) for applications involving exposure to moderately elevated temperature (up to ca. 200°C). The ZE63 alloy is a high-strength variant in which solution heat treatment in a hydrogen atmosphere is employed to remove some of the embrittling Mg-Zn-RE grain boundary phases. In extrusion, microporosity

is of less concern and Mg-Zn-Zr alloys are used without RE additions [9-13, 27].

Mg-Ag-RE-Zr. Addition of silver and neodymium-rich misch metal, in addition to zirconium, promotes age hardening efficiently when the alloy is given a full T6 treatment (solution heat-treated and artificially aged). The precipitates formed are relatively stable; the alloy shows high mechanical strength and good creep properties at temperatures approaching 250°C [9, 26].

Mg-Y-RE-Zr. The most recently developed alloy system for high-temperature application is based upon additions of yttrium and neodymium-rich misch metal. This alloy system was developed to meet the ever-increasing high-temperature performance requirements of the aerospace industry and may replace the Mg-Ag-RE-Zr and thorium-containing alloys. The alloys must be melted in a special inert atmosphere (argon) and develop their properties by T6 heat treatment [10].

This work present an influence of Al concentration and cooling rate on structure and mechanical properties of magnesium alloys. Also the paper presents a methodology to predict crystallization temperatures obtained during crystallization process using an UMSA platform, based on cooling rate and chemical composition and mechanical properties and grain size based on characteristics temperatures.

2. Experimental procedure

2.1. Material

The investigations have been carried out on test pieces of MC MgAl12Zn1, MC MgAl9Zn, MC MgAl6Zn1, MC MgAl3Zn magnesium alloys in as-cast and after heat treatment states made in cooperation with the Faculty of Metallurgy and Materials Engineering of the Technical University of Ostrava and the CKD Motory plant, Hradec Kralove in the Czech Republic. The chemical compositions of the investigated materials are given in Table 2. A casting cycle of alloys has been carried out in an induction crucible furnace using a protective salt bath *Flux 12* equipped with two ceramic filters at the melting temperature of 750±10ºC, suitable for the manufactured material. In order to maintain a metallurgical purity of the melting metal, a refining with a neutral gas with the industrial name of *Emgesalem Flux 12* has been carried out. To improve the quality of a metal surface a protective layer *Alkon M62* has been applied. The material has been cast in dies with betonite binder because of its excellent sorption properties and shaped into plates of 250x150x25. The cast alloys have been heated in an electrical vacuum furnace *Classic 0816 Vak* in a protective argon atmosphere.

Table 2.
Chemical composition of investigated magnesium alloys

The mass concentration of main elements, %						
Al	Zn	Mn	Si	Fe	Mg	Rest
12.1	0.62	0.17	0.047	0.013	86.96	0.0985
9.09	0.77	0.21	0.037	0.011	89.79	0.0915
5.92	0.49	0.15	0.037	0.007	93.33	0.0613
2.96	0.23	0.09	0.029	0.006	96.65	0.0361

2.2. Test sample

The experiments were performed using a pre-machined cylindrical test sample with a diameter of ∅=18mm and length of l=20mm taken from the ingot (Fig. 2). In order to assure high repeatability and reproducibility of the thermal data, the test sample mass was ≈9.2g. Each sample had a predrilled hole to accommodate a supersensitive K type thermocouple (with extra low thermal time constants) positioned at the centre of the test sample to collect the thermal data and control the processing temperatures.
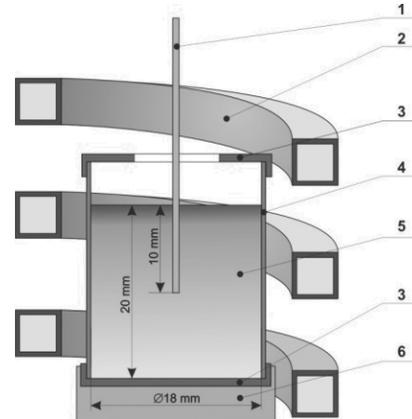

Fig. 2. Schematic of the UMSA Thermal Analysis Platform experimental set-up: 1 – low thermal mass thermocouple, 2 – heating and cooling coil, 3 – thermal insulation, 4 – steel foil, 5 – test sample, 6 – ceramic base

2.3. Thermal analysis

The thermal analysis during melting and solidification cycles was carried out using the Universal Metallurgical Simulator and Analyzer (UMSA) (Fig. 3) [28, 29]. The melting and solidification experiments for the magnesium alloys were carried out using Argon as cover gas. The data for Thermal Analysis (TA) was collected using a high-speed National Instruments data acquisition system linked to a personal computer. Each TA trial was repeated three times.

The TA signal in the form of heating and cooling curves was recorded during the melting and solidification cycles. The temperature vs. time and first derivative vs. temperature were calculated and plotted. The cooling rates for these experiments were determined using the following formula [18]:

$$CR = \frac{T_{liq} - T_{sol}}{t_{sol} - t_{liq}} \quad \left[\frac{°C}{s} \right] \tag{1}$$

were T_{liq} and T_{sol} are the liquidus and solidus temperatures (°C), respectively, and t_{liq} and t_{sol} the times from the cooling curve that correspond to liquidus and solidus temperatures, respectively [16, 17].

The procedure comprised of the following steps. First, the test sample was heated to 700±2°C and isothermally kept at this temperature for a period of 90s in order to stabilize the melt

conditions. Next, the test sample was solidified at cooling rate of approximately 0.6°C/s, that was equivalent to the solidification process under natural cooling conditions. To achieve an intentional cooling rate:

- 0.6°C/s sample was cooled without forces air
- 1.2°C/s sample was cooled in airflow 30 l/min,
- 2.4°C/s sample was cooled in airflow 125 l/min.
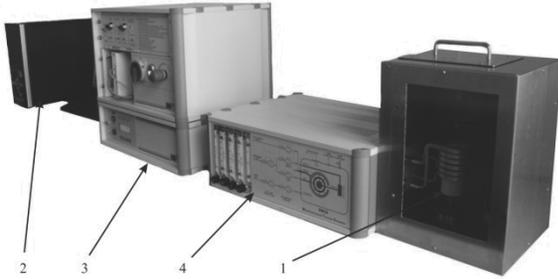
Fig. 3. UMSA apparatus - (1) sample chamber, (2) supervisory computer, (3) temperature control, (4) gas flow control

Fraction solid (FS) was determined by calculating the cumulative surface area between the first derivative of the cooling curve and the so-called base line (BL) [19, 20]. The BL represents the hypothetical first derivative of the cooling curve that does not exhibit phase transformation/metallurgical reactions during the solidification process. The area between the two derivative curves (calculated between the liquidus and solidus temperatures) is proportional to the latent heat of solidification of the given alloy. Therefore, the latent heat directly delivered to the test sample affected the fraction liquid evolution. Similar calculations were performed for the fraction solid except that fraction solid was proportional to the latent heat released during the solidification [14, 15].

The magnesium nucleation temperature T_N, T_{Dmin}, T_{DKP}, T_G, $T_{(Mg+Si+Al+Mn)}$, $T_{E(Mg+Al)N}$, $T_{E(Mg+Al)min}$, $T_{E(Mg+Al)G}$ and solidus temperatures T_{sol}, where calculated using the first derivative of the cooling curve [30].

The α-Mg Dendrite Nucleation Temperature, ($T^{\alpha DEN}_{NUC}$) represents the point at which primary stable dendrites start to solidify from the melt. This event is manifested by the change in the slope of the cooling curve and determined by the first derivative inflection point. The liquidus temperature signifies the beginning of the fraction solid that, at this point, is equal to zero.

The α-Mg Dendrite Minimum (Undercooling) Temperature, ($T^{\alpha DEN}_{MIN}$) represents a state where the nucleated dendrites have grown to such an extent that the liberated latent heat of fusion balances the heat extracted from the test sample. After passing this point, the melt temperature increases to a steady state growth temperature ($T^{\alpha DEN}_G$). $T^{\alpha DEN}_{NUC}$ as the local minimum is determined at the point at which the first derivative intersects the zero line (dT/dt=0). The time period required for heating up of the test sample to the $T^{\alpha DEN}_G$ is called recalescence [30].

At the start of solidification of a melt, small equiaxed crystals are developing, separate from one another. The viscosity of the melt and hence torque is very small. As the dendrites grow in size and start to impinge upon one another, a continuous solid network builds up throughout the sample volume. There is a sudden increase in the torque force needed to shear the solid network. This point is called "coherency point".

The α-Mg Dendrite Growth Temperature, ($T^{\alpha DEN}_G$) represents the local maximum temperature of this reaction (and is also called the "steady state growth temperature). The $T^{\alpha DEN}_G$ corresponds to the second zero point on the first derivative curve (dT/dt=0) following the start of nucleation (dT/dt = 0). If the first derivative curve in this region does not intersect the zero line, $T^{\alpha DEN}_{MIN}$ the $T^{\alpha DEN}_G$ temperatures are identical and correspond to the maximum point on the first derivative curve (Figs. 4-6 and Table 3) [14, 15, 30].
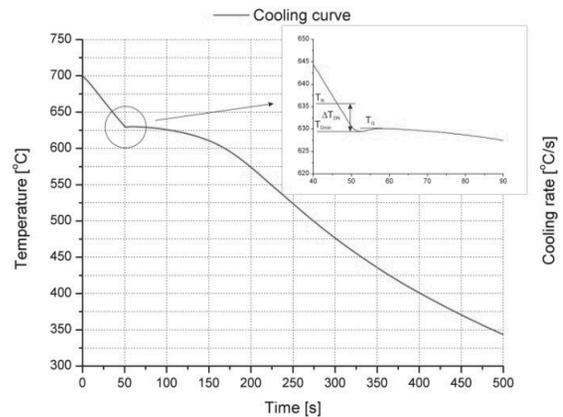

Fig. 4. Cooling curve of MC MgAl3Zn1 alloy obtained under non-equilibrium experimental condition: ΔT_{DN} nucleation undercooling

The shape of the cooling curve is the result of the heat lost to the surroundings by the cooling metal and the heat evolved in the melt during phase transformation. At the beginning of solidification of any phase, the derivative increases in value, and decreases at the end of solidification [21-24].
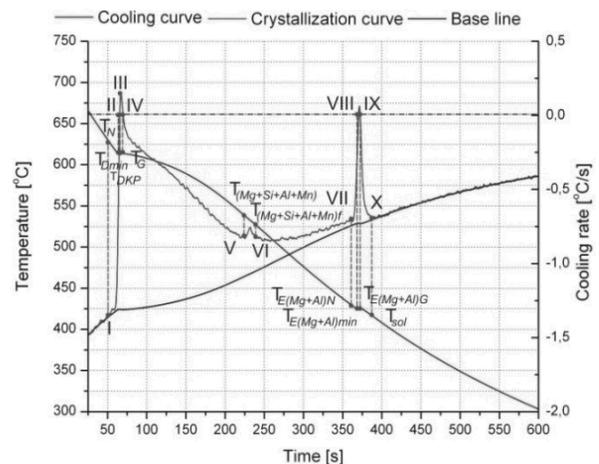

Fig. 5. Representative cooling, crystallization and calorimetric curves with characteristics points of crystallization process of MC MgAl6Zn1 alloy cooled at 0.6°C/s

Based on characteristics points from the thermal analysis, heat of phase transition individual phases was calculated. Temperatures and times of thermal processes were calculated as well. Heat capacity of the alloy was determined using the following formula [16, 17]:

$$c_p(t) = c_{psol} \cdot \int_{t_N}^{t} f_s(t)dt + c_{psol} \cdot (1 - \int_{t_N}^{t} f_s(t)dt) \qquad (2)$$

where: f_s – participation of fraction solid, considering that for f_s $(t \leq t_N)= 0$ and $f_s(t \geq t_N)= 1$. Thermal-Calc Software was used to determine a specific heat capacity in liquid and solid state. Total heat of crystallization process of analyzed alloys was calculated based on:

$$Q = c_p \cdot m \cdot \int_{t_N}^{t_{sol}} \left[\frac{dT}{dt} - \left(\frac{dT}{dt} \right)_c \right] \qquad (3)$$
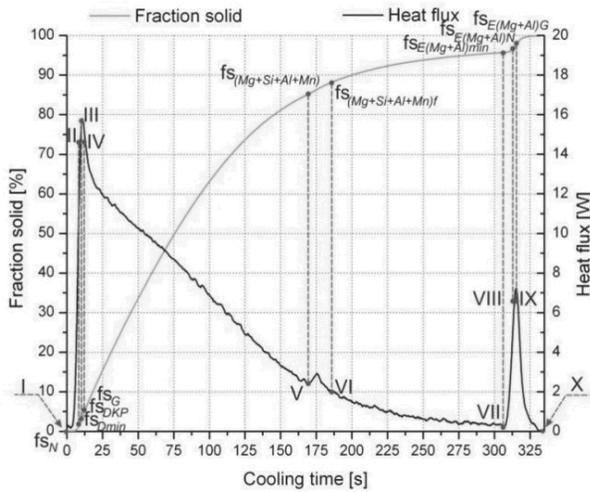
Fig. 6. Representative curves illustrate changes of heat flux and fraction solid of MC MgAl6Zn1 alloy cooled at 0.6°C/s

2.4. Microstructure examinations

Metallographic samples were taken from a location close to the thermocouple tip. Samples were cold mounted and grounded on 240, 320, 400, 600 and 1200 grit SiC paper and then polished with 6μm, 3μm and 1μm diamond paste. The polished surfaces were etched with a solution of 2g oxalic acid, 100ml water, with fresh alcohol blotted repeatedly onto the surface to prevent residue deposits. The observations of the investigated cast materials have been made on the light microscope LEICA MEF4A as well as on the electron scanning microscope Opton DSM-940.

The X-ray qualitative and quantitative microanalysis and the analysis of a surface distribution of cast elements in the examined magnesium cast alloys have been made on the Opton DSM-940 scanning microscope with the Oxford EDS LINK ISIS dispersive radiation spectrometer at the accelerating voltage of 15 kV. Phase composition and crystallographic structure were determined by the X-ray diffraction method using the XPert device with a copper lamp, with 40 kV voltage. The measurement was performed by angle range of 2θ: 30º - 120º.

Observations of thin foil structure were carried out in the JEM 3010UHR JEOL transmission electron microscope using an accelerating voltage of 300 kV.

2.5. Mechanical properties

Samples for compression testing were machined from a centre of the thermal analyses specimen ingots. The machined samples were polished with fine sandpaper to remove any machining marks from the surface. Compression tests were conducted at room temperature using a Zwick universal testing machine. Prior to testing, an extensometer was used to minimize frame bending strains. Compression specimens were tested corresponding to each of the three cooling rates.

Rockwell F–scale hardness tests were conducted at room temperature using a Zwick HR hardness testing machine.

2.6. Data collection and database construction

The performance of an ANN model depends upon the dataset used for its training. Therefore, for a reliable neural network model a significant amount of data as well as powerful computing resources are necessary [33-37].

Table 3.
Characteristic points obtained from thermal-derivative analysis

Point	Temperature	Time	Description
I	T_N	t_N	Nucleation of α-phase (liquidus temperature)
II	T_{Dmin}	t_{Dmin}	The α-Mg dendrite minimum (undercooling) temperature
III	T_{DKP}	t_{DKP}	Coherency point
IV	T_G	t_G	The α-Mg dendrite growth temperature
V	$T_{(Mg+Si+Al+Mn)}$	$t_{(Mg+Si+Al+Mn)}$	Crystallization of α-Mg, Mg_2Si and phases contains Al and Mn
VI	$T_{(Mg+Si+Al+Mn)f}$	$t_{(Mg+Si+Al+Mn)f}$	End of crystallization of Mg_2Si and phases contains Al and Mn
VII	$T_{E(Mg+Al)N}$	$t_{E(Mg+Al)N}$	Beginning of nucleation of α(Mg)-γ $(Mg_{17}Al_{12})$ eutectic
VIII	$T_{E(Mg+Al)min}$	$t_{E(Mg+Al)min}$	The α(Mg)- γ $(Mg_{17}Al_{12})$ minimum (undercooling) temperature
IX	$T_{E(Mg+Al)G}$	$t_{E(Mg+Al)G}$	The α(Mg)- γ $(Mg_{17}Al_{12})$ eutectic growth temperature
X	T_{sol}	t_{sol}	End of solidification (solidus temperature)

Amounts of data on mechanical properties of magnesium alloys at different conditions are currently available in the literature [31, 32].

However, these data are rather disordered and confusing for the use of engineering practice. Moreover, in Mg-system, the experimental data in the literature are very sparse compared to Al-alloys and steels.

The gathered set of data designed for formation of a numerical model determining: UCS, HRF and GS in relation to the chemical composition and cooling rate were divided into two subsets: the learning set and the validation set. The data were divided in a proportion of 75% for the learning set and 25% for the validation set. For data analysis four neural networks models were used:

- multilayer perceptron MLP,
- linear neural networks,
- radial basis functions neural network RBF,
- generalized regression neural networks GRNN,

also the following learning methods:

- back propagation method,
- conjugate gradient,
- quasi-Newtona method,
- fast propagation.

3. Results and discussion

3.1. Thermal analysis

Representative thermal analysis of the magnesium alloys have been presented in Figure 4. Three visible temperature arrests were noted on the cooling curves. More detailed information pertaining to the alloy's thermal characteristics such as non-equilibrium liquidus, nucleation of the α(Mg)-γ(Mg$_{17}$Al$_{12}$) eutectic, etc. were determined using the first derivative curves.

An example of the cooling and crystallization curve of the Mg-Al-Zn alloy cooled with different cooling rates are presented in Figures 7 and 8.
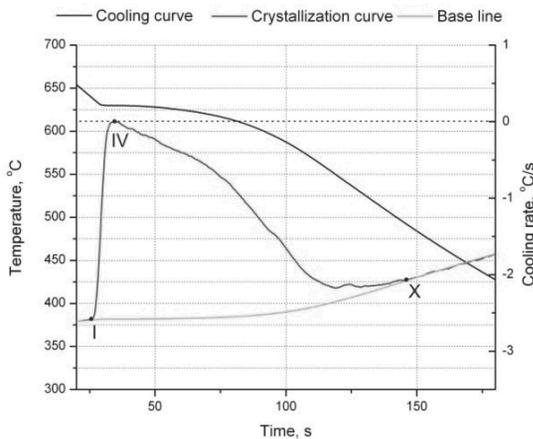
Fig. 7. Representative cooling and crystallization curves of MC MgAl3Zn1 magnesium alloys cooled at 1.2°C/s

a)
b)
c)
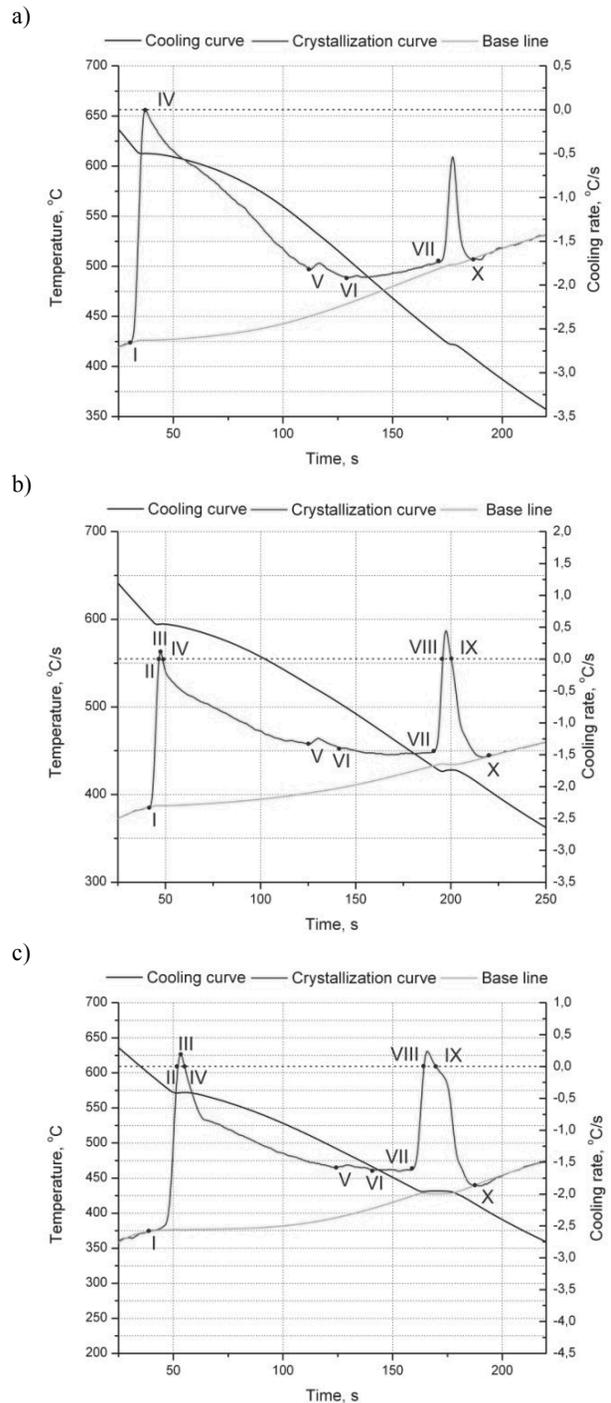
Fig. 8. Representative cooling and crystallization curves of magnesium alloys cooled at 1.2°C/s, a) MC MgAl6Zn1, b) MC MgAl9Zn1, c) MC MgAl12Zn1

The performed crystallization process analysis on the basis of the achieved curves allows it to state, that the nucleation process of the α phase begins at the T_{DN} temperature. This effect is present on the curve in form of an inflexion in point I,

as well in form of an instantaneous decrease of the cooling rate. Decrease of the crystallisation rate of the remaining liquid metal is caused by the heat provided from the α phase nuclei, which is smaller compared to the heat amount submit into the surrounding by the solidified metal. This process ends in point II, where the crystallization temperature achieves the minimal value - T_{Dmin}, where the α phase crystals begins to growth. In this point the derivative value achieves the zero value. The cooled alloy, resulting in crystallisation heat emission, reheats the remaining liquid until the T_{DKP} (point III) temperature. The further crystal growth causes an increase of the temperature of the remaining liquid to the maximal crystallisation temperature of the α phase – T_G (point IV).

Table 4.
Non-equilibrium characteristics of the MC MgAl3Zn1 alloy

Point	Cooling rate, °C/s		
	0.6	1.2	2.4
	Temperature, °C	Temperature, °C	Temperature, °C
I	633.16	635.39	640.32
II	630.44	Not observed	Not observed
III	630.64	Not observed	Not observed
IV	630,85	630.42	629.71
V	Not observed	Not observed	Not observed
VI	Not observed	Not observed	Not observed
VII	Not observed	Not observed	Not observed
VIII	Not observed	Not observed	Not observed
IX	Not observed	Not observed	Not observed
X	508.96	502.03	492.28

Table 5.
Non-equilibrium characteristics of the MC MgAl6Zn1 alloy

Point	Cooling rate, °C/s		
	0.6	1.2	2.4
	Temperature, °C	Temperature, °C	Temperature, °C
I	615.88	615.74	619.77
II	611.51	Not observed	Not observed
III	611.75	Not observed	Not observed
IV	611.92	610.33	608.14
V	533.65	532.77	536.37
VI	520.18	509.72	511.99
VII	429.45	431.69	432.99
VIII	426.59	Not observed	Not observed
IX	427.17	Not observed	Not observed
X	419.47	415.44	401.66

Further alloy cooling causes the beginning of crystallisation of the silicon, aluminium and manganese- rich phases, which are emitting an additive heat amount present on the crystallisation curve in form of clear heat effect – described as $T_{(Mg+Si+Al+Mn)}$ and $T_{(Mg+Si+Al+Mn)f}$ (points V and

VI). As a result of further alloy cooling after reaching the $T_{E(Mg+Al)N}$ temperature there occurs the nucleation of the α+γ eutectic (point VII). The cooled alloy reach the $T_{E(Mg+Al)min}$ (point VIII) temperature, as next the temperature increases until the maximum crystallisation temperature of the eutectic $T_{E(Mg+Al)G}$ (point IX). The alloy crystallisation ends in point X, where the T_{sol} value is reached. The temperatures of the metallurgical reactions are presented in Tables 4-7.

Table 6.
Non-equilibrium characteristics of the MC MgAl9Zn1 alloy

Point	Cooling rate, °C/s		
	0.6	1.2	2.4
	Temperature, °C	Temperature, °C	Temperature, °C
I	597.97	600.74	600.89
II	592.29	593.02	Not observed
III	592.65	593.27	Not observed
IV	592.91	592.79	592.01
V	515.8	524.28	524.43
VI	503.07	504.96	502.88
VII	428.78	429.5	433.71
VIII	425.76	424.76	Not observed
IX	427.25	425.83	Not observed
X	413.01	412.19	404.11

Table 7.
Non-equilibrium characteristics of the MC MgAl12Zn1 alloy

Point	Cooling rate, °C/s		
	0.6	1.2	2.4
	Temperature, °C	Temperature, °C	Temperature, °C
I	580.76	583.51	586.2
II	572.92	572.09	Not observed
III	573.22	572.49	Not observed
IV	576.03	572.87	575.09
V	491.36	492.58	497.22
VI	481.74	476.63	476.44
VII	433.03	435.69	438.75
VIII	430.58	430.15	Not observed
IX	432.57	431.92	Not observed
X	420.86	416.11	417.04

In Figures 9 and 10 there are presented the solid state fraction change as well the heat flux generated by the crystallised phases. This information is used for determination of the crystallising heat emitted by the particular phases (Tables 8-11). In Figure 11 is presented the influence of the cooling rate as well the magnesium content on the temperature - T_{DN} of the α phase nucleation. On the basis of the performed investigation it was found that the biggest influence on the nucleation temperature has the aluminium content (it decreases the nucleation temperature of the α phase according

to the liquidus line) as well the cooling rate (it causes an increase of the α phase nucleation temperature). For example for the MC MgAl3Zn1 alloy an increase of the cooling rate from 0.6 to 1.2°C/s causes an increase of the α phase nucleation temperature from 633.16 to 635.39°C, further increase of the cooling rate until 2.4°C/s causes a temperature growth until 640.32°C.

Table 8.
Latent heat of crystallization process emitted during solidification of MC MgAl3Zn1

Reaction	Cooling rate, °C/s		
	0.6	1.2	2.4
L→ α(Mg)	1400.96	1422.31	1392.02
L→ α(Mg)+ +Mg$_2$Si+(Al+Mn)	Not observed		
L→ α(Mg)+γ(Mg$_{17}$Al$_{12}$)			
sum	1400.96	1422.31	1392.02

Table 9.
Latent heat of crystallization process emitted during solidification of MC MgAl6Zn1

Reaction	Cooling rate, °C/s		
	0.6	1.2	2.4
L→ α(Mg)	1258.22	1255.55	1390
L→ α(Mg)+Mg$_2$Si+(Al+Mn)	143.63	131.32	161.17
L→ α(Mg)+γ(Mg$_{17}$Al$_{12}$)	55.98	56.86	107.71
sum	1457.84	1443.74	1658.88

Table 10.
Latent heat of crystallization process emitted during solidification of MC MgAl9Zn1

Reaction	Cooling rate, °C/s		
	0.6	1.2	2.4
L→ α(Mg)	1180.37	1153.43	1213.15
L→ α(Mg)+ +Mg$_2$Si+(Al+Mn)	273.84	302.22	289.91
L→ α(Mg)+γ(Mg$_{17}$Al$_{12}$)	172.39	183.41	195.91
sum	1626.6	1639.09	1698.98

Table 11.
Latent heat of crystallization process emitted during solidification of MC MgAl12Zn1

Reaction	Cooling rate, °C/s		
	0.6	1.2	2.4
L→ α(Mg)	985.47	1113.78	1029.97
L→ α(Mg)+Mg$_2$Si+(Al+Mn)	200.47	221.56	216.07
L→ α(Mg)+γ(Mg$_{17}$Al$_{12}$)	246.05	349.35	270.17
sum	1432	1684.7	1516.21

a)

b)

c)
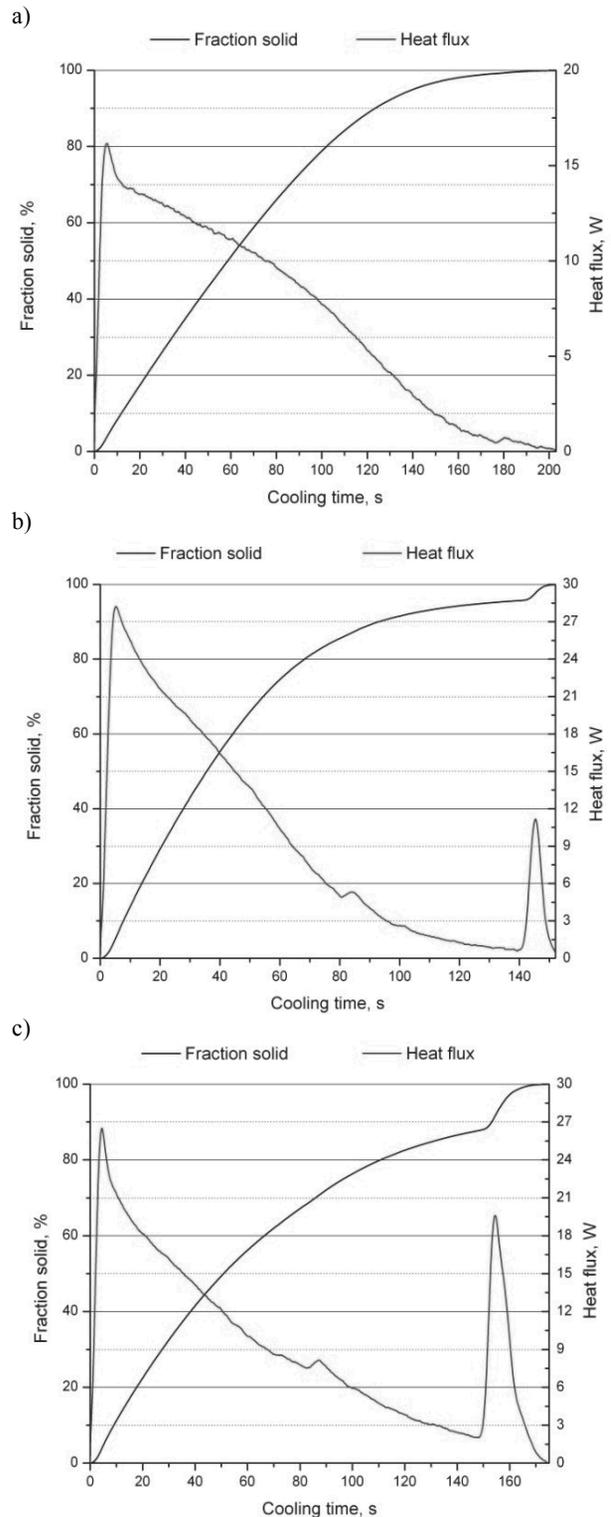
Fig. 9. Representative curves illustrate changes of heat flux and fraction solid of magnesium alloys cooled at 1.2°C/s, a) MC MgAl3Zn1, b) MC MgAl6Zn1, c) MC MgAl9Zn1
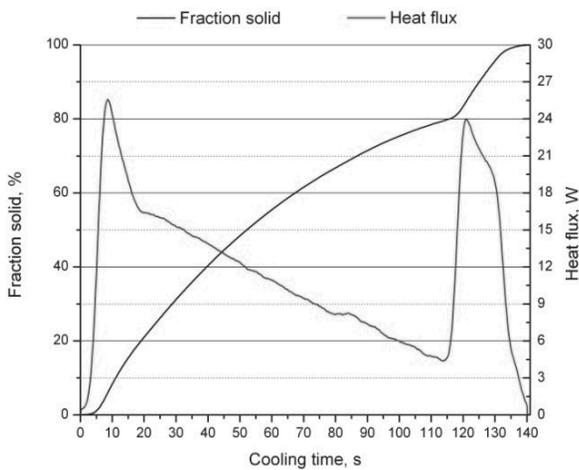
Fig. 10. Representative curves illustrate changes of heat flux and fraction solid of MC MgAl12Zn1 magnesium alloys cooled at 1.2°C/s


Fig. 12. Influence of cooling rate and aluminium concentration on dendrite growth temperature
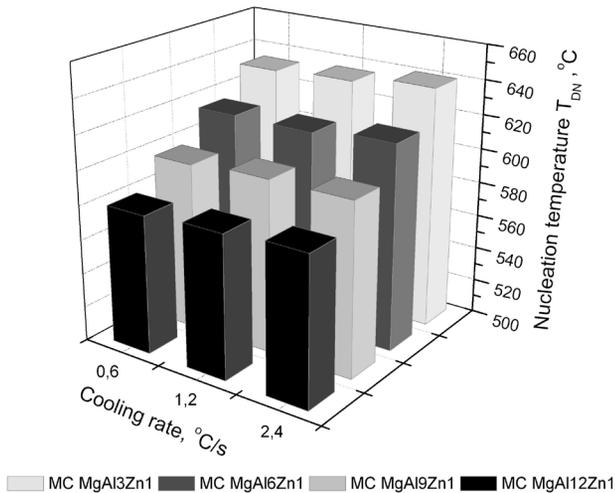
Fig. 11. Influence of cooling rate and aluminium concentration on nucleation temperature

In Figure 12 there is presented the influence of the magnesium mass concentration as well the cooling rate on the maximal crystallization temperature (T_G) of the α phase. On the basis of the performed investigation it was found that the change of the cooling rate does not influence the maximal crystallization temperature (T_G) of the α phase. It was also found that the T_G temperature decreases together with the increase of the aluminium content. For example for the alloys cooled with a rate of 0.6°C/s, the increase of aluminium content from 3 to 6% causes a decrease of the maximal crystallization temperature of the α phase from 630.85 to 611.92°C, and a further increase of the aluminium content of 9% causes a decrease of the temperature value to 592.91°C. The lowest values of the maximal α phase crystallization temperature - equal 576.03°C, was observed for the alloy with 12% aluminium content.
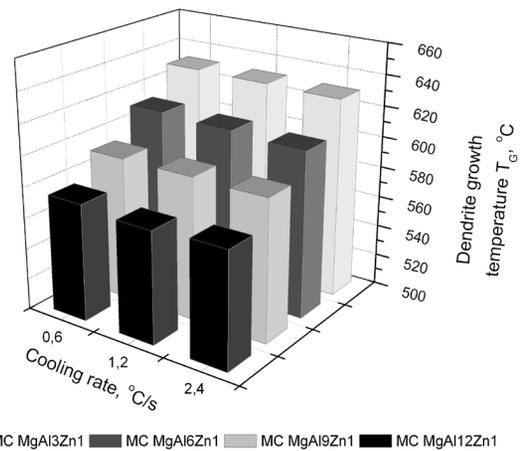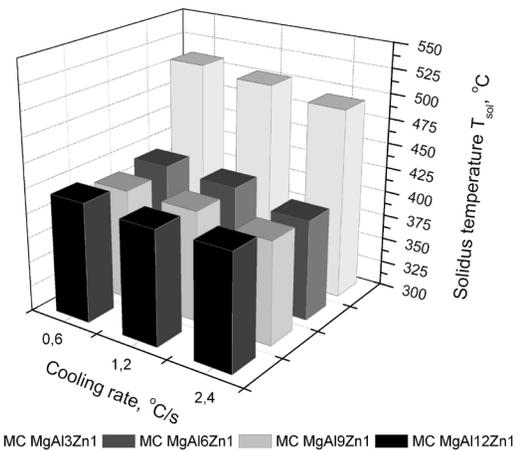
Fig. 13. Influence of cooling rate and aluminium concentration on dendrite growth temperature
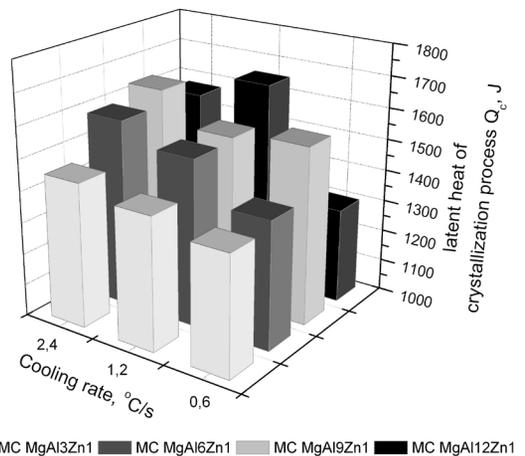
Fig. 14. Influence of cooling rate and aluminium concentration on latent heat of crystallization process

Figure 13 presents an influence of aluminium mass concentration and cooling rate on solidus temperature. On the basis of the performed investigation it was found that the biggest influence on the nucleation temperature has the aluminium content (it increases the solidus temperature) as well the cooling rate (it causes an decrease of the solidus temperature).

In Figure 14 there is presented the influence of cooling rate as well the influence of aluminium mass content on the heat amount emitted during the alloy crystallisation. On the basis of the performed calculations it was found, that the biggest influence on the heat (Q_c) increase generating during alloy crystallization has the variable aluminium content. An increase of thee aluminium content in the investigated alloys causes an increase of the heat Q_c. In case of an increase of the cooling rate there was observed a small growth of the generating crystallization heat except the MC MgAl3Zn1 alloy.

3.2. Microstructure characterization

The analysis of thin foils (Figs. 15-17) after thermal analysis has validated the fact that the structure of the magnesium cast alloy consists of the solid solution α – Mg (matrix) and an intermetallic secondary phase γ – Mg$_{17}$Al$_{12}$ in the form of needle precipitations (Figs. 15, 17).

a)
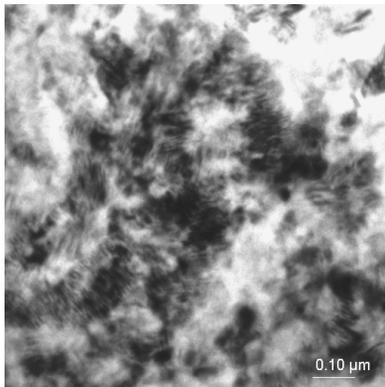
b)
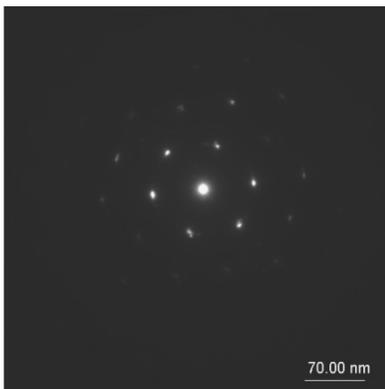
Fig. 15. TEM image of the MC MgAl6Zn1 alloy cooled at 0.6°C/s a) bright field; b) diffraction pattern of area shown in a)
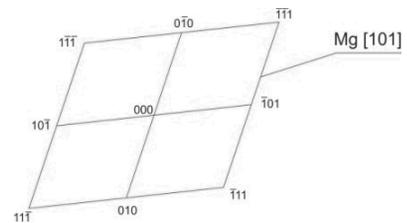
Fig. 16. Part of solution for diffraction pattern shown in Fig. 15b

a)
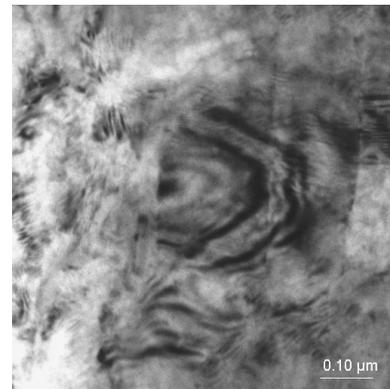
b)
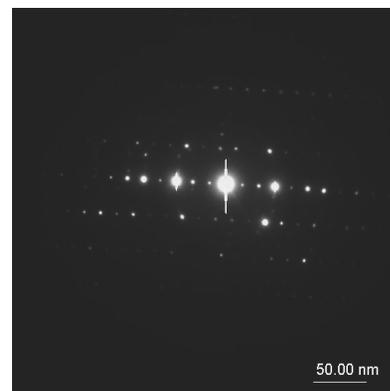
c)
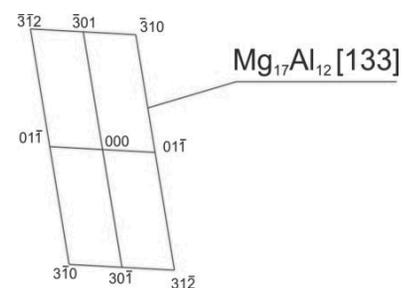
Fig. 17. TEM image of the MC MgAl9Zn1 alloy cooled at 0.6°C/s a) bright field; b) diffraction pattern of area shown in a), c) part of solution for diffraction pattern shown in b

According to the X–ray phase analysis, the investigated magnesium alloys cooled with solidification rate: 0.6, 1.2 and 2.4. °C/s is composed of two phases (Fig. 18): α–Mg solid solution as matrix and γ(Mg$_{17}$Al$_{12}$). In the diffraction pattern

of the matrix, the {011} Mg–diffraction line has very intensity. Based on the X–ray phase analysis was found, that change of solidification rate don't influence on the phases composition of investigated alloy. The X–ray phase analysis don't ravel occurring of Mg_2Si and phases contains Mn and Al, what suggested that the fraction volume of these phases is below 3%.
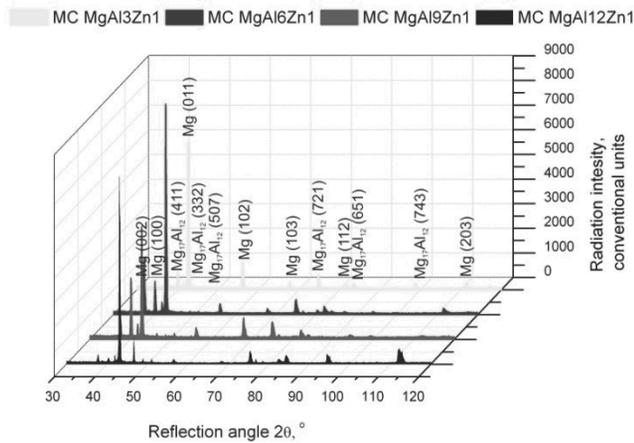

Fig. 18. XRD pattern of magnesium alloys at natural cooling

The general microstructure after thermal analysis revealed the presence of dendrite of solid solution of Al in Mg (α-phase) and divorced eutectic structure made of Al-rich Mg solid solution and $Mg_{17}Al_{12}$ (γ-phase). Moreover, angular particles of Mg_2Si and globular particles of phases contains Al and Mn mainly located at interdendritic spaces were observed (Figs. 19, 20). This observation was in agreement with thermal analysis experiments where three distinct metallurgical reactions were noted on the cooling curve, i.e., nucleation of the α(Mg), the Mg_2Si and the α(Mg)+γ($Mg_{17}Al_{12)}$ eutectic.
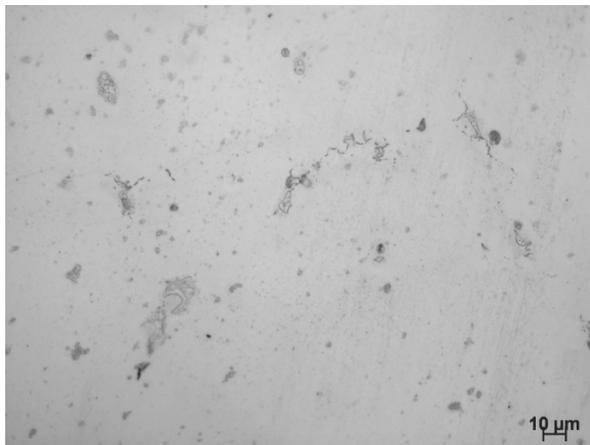
Fig. 19. Microstructure of MC MgAl3Zn1 magnesium alloy cooled at 1.2°C/s, mag. 500x

a)

b)

c)
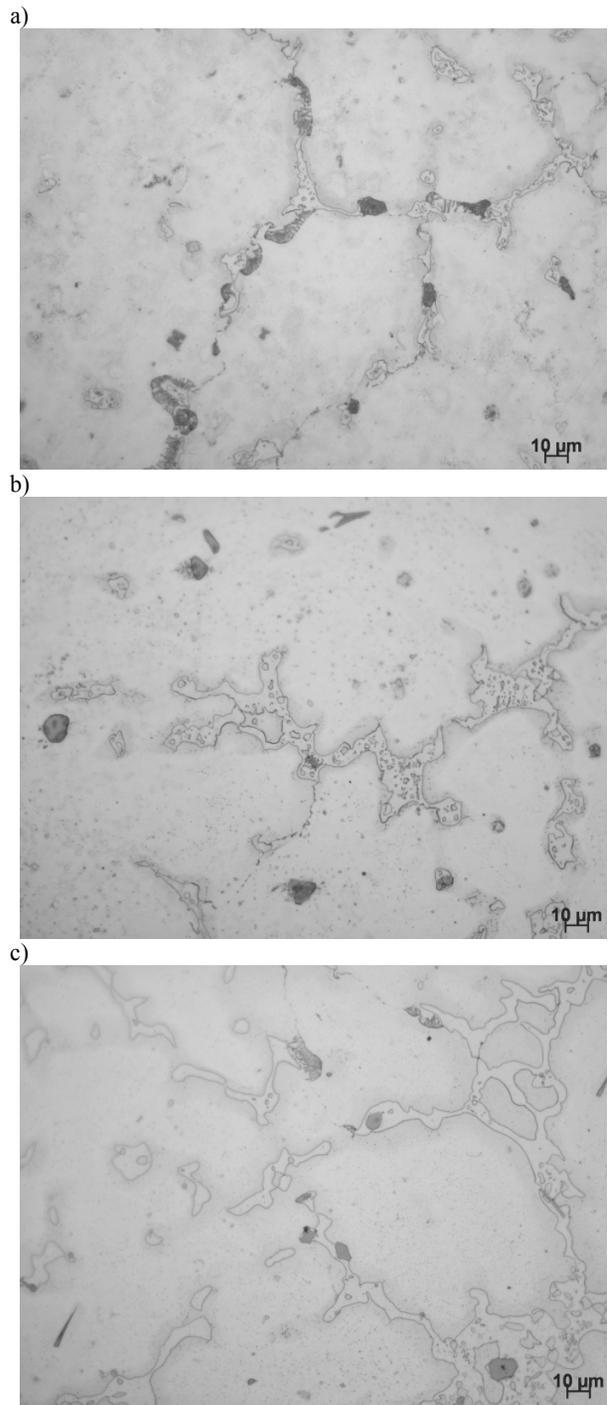
Fig. 20. Microstructure of magnesium alloys cooled at 1.2°C/s, a) MC MgAl6Zn1, b) MC MgAl9Zn1, c) MC MgAl12Zn1, mag. 500x

The carried out investigations revealed, that the grain size decreases together with the cooling rate increase for each of the analysed alloys. On the basis of the performed investigations it was found that the largest grain size is

characteristic for the MC MgAl6Zn1 alloy. A cooling rate change from 0.6 to 2.4°C/s causes a two times decrease of the grain size. A similar dependence was found also for other analysed alloys, which were studied in this investigation. An increase of the aluminium mass concentration causes a slightly decrease of the grain size (Fig. 21).
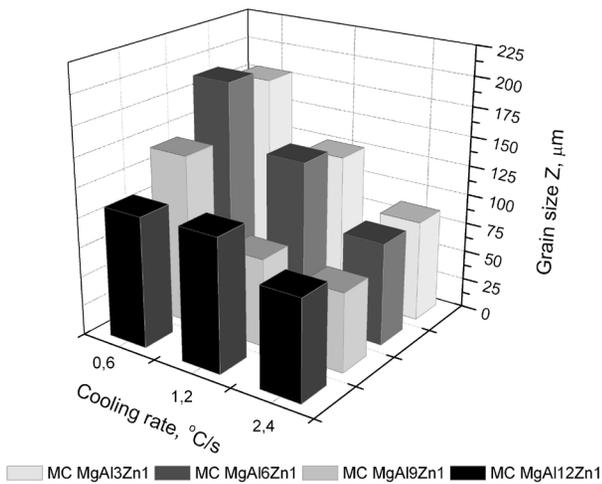

Fig. 21. Influence of cooling rate and aluminium concentration on grain size of analyzed cast magnesium alloys

Representative SEM micrographs of magnesium alloys cooled at 1.2°C/ are shown in Figures 22, 23. Results from EDS analysis are shown in Tables 12-15. EDS spectra for all samples confirms that, the matrix is α-Mg, and intermetallics phases mostly likely Mg_2Si, and Al-Mn (it could be a mixture of Al_8Mn_5 or $MnAl_4$). Because the size of particular elements of the structure is, in a prevailing measure, smaller than the diameter of the analyzing beam, the obtained at the quantitative analysis chemical composition may be averaged as a result of which some values of element concentrations may be overestimated.
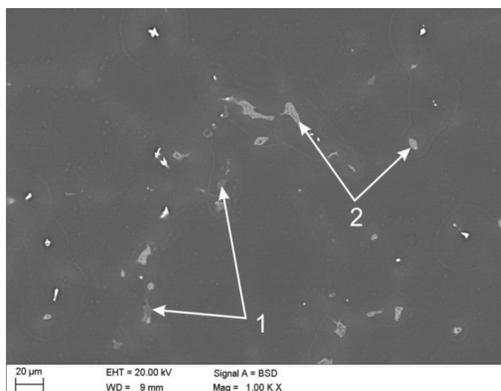

Fig. 22. Representative scanning electron microscope micrograph of MC MgAl3Zn1 magnesium alloy that solidified with cooling rate 1.2°C/s

a)

b)

c)
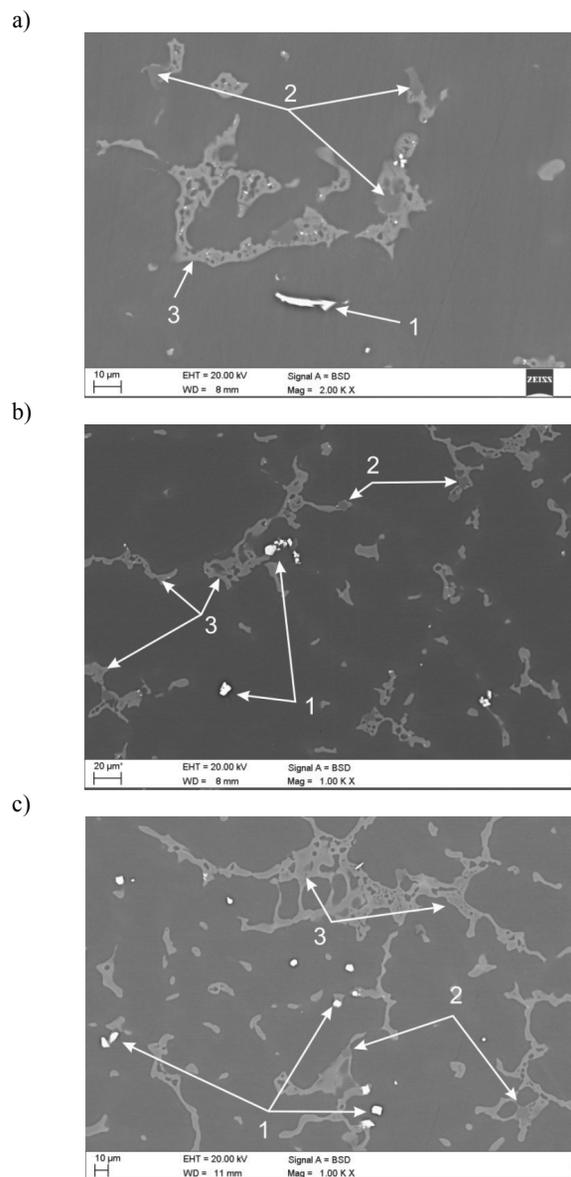
Fig. 23. Representative scanning electron microscope micrographs of magnesium alloy that solidified with cooling rate 1.2°C/s: a) MC MgAl6Zn1, b) MC MgAl9Zn1, c) MC MgAl12Zn1

Table 12.
Pointwise chemical composition analysis from Fig. 22

	Element	The mass concentration of main elements, %	
		weight %	atomic %
1	Mg	74.14	76.8
	Si	25.86	23.2
2	Zn	4.12	1.6
	Mg	78.63	82.16
	Al	17.25	16.24

Table 13.
Pointwise chemical composition analysis from Fig. 23a

Element		The mass concentration of main elements, %	
		weight %	atomic %
1	Mg	10.29	15.33
	Al	36.12	48.48
	Si	1.36	1.75
	Mn	52.23	34.43
2	Mg	66.6	69.73
	Si	33.4	30.27
3	Zn	6.03	2.41
	Mg	62.4	67.03
	Al	31.58	30.56

Table 14.
Pointwise chemical composition analysis from Fig. 23b

Element		The mass concentration of main elements, %	
		weight %	atomic %
1	Mg	12.41	17.27
	Al	45.05	56.51
	Mn	42.55	26.22
2	Zn	7.44	3.01
	Mg	66.16	72.08
	Si	26.4	24.9
3	Mg	66.42	70.15
	Al	29.81	28.37
	Zn	3.77	1.48

Table 15.
Pointwise chemical composition analysis from Fig. 23c

Element		The mass concentration of main elements, %	
		weight %	atomic %
1	Mg	1.57	2.38
	Al	45.17	61.82
	Mn	53.26	35.8
2	Mg	66.06	69.22
	Si	33.94	30.78
3	Zn	3.75	1.48
	Mg	61.58	65.36
	Al	34.68	33.16

Figure 24 presents a chemical analysis of the surface element decomposition.
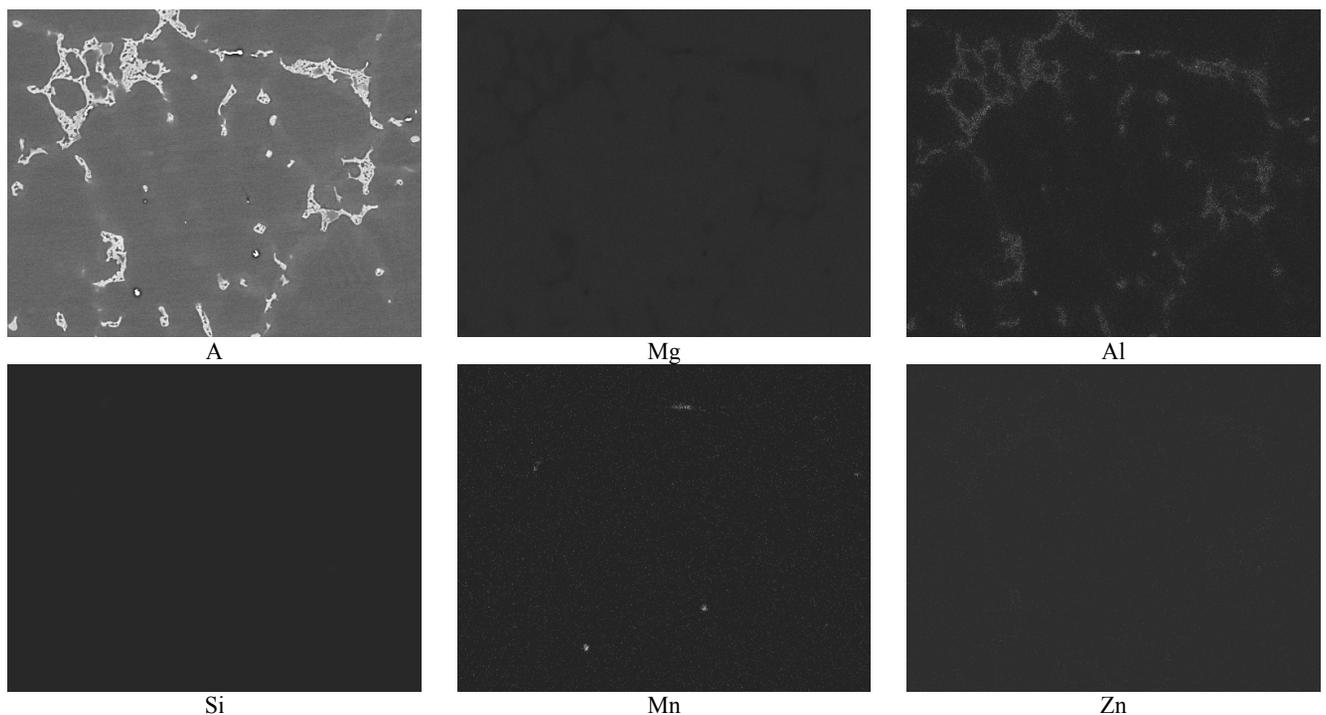
Fig. 24. The area analysis of chemical elements alloy MC MgAl6Zn1 cooled at 1.2°C/s cooling rate: image of secondary electrons (A) and maps of elements' distribution

3.3. Mechanical properties

Figure 25 shows the influence of aluminium mass concentration as well the cooling rate on hardness of the investigated alloys. On the basis of the performed investigations it was found a linear increase of the hardness compared to the increase of the aluminium content, and also an increase of the cooling rate for the MC MgAl6Zn1, MC MgAl9Zn1 and MC MgAl12Zn1 alloy. For the MC MgAl3Zn1 alloy it was found a hardness increase up to 26 HRF by a cooling rate of 1.2°C/s. A cooling rate increase up to 2.4°C/s causes a decrease of the hardness down to 19 HRF. The highest hardness value of 74 HRF was achieved for the MC MgAl12Zn1 alloy cooled with a rate of 2.4°C/s.
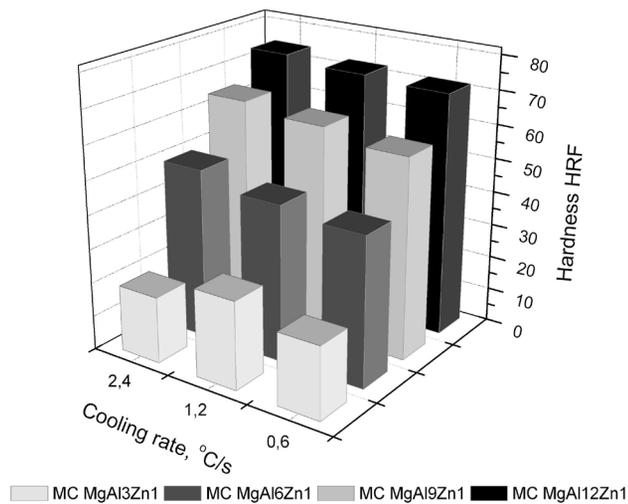
Fig. 25. Influence of cooling rate and aluminium concentration on hardness
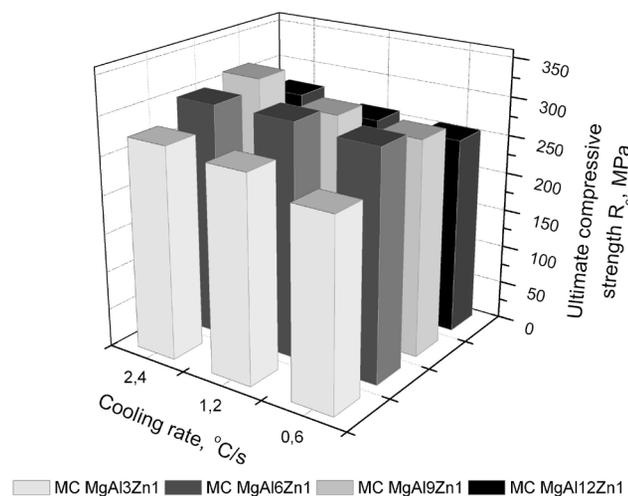

Fig. 26. Influence of cooling rate and aluminium concentration on ultimate compressive strength of cast magnesium alloys

Figure 26 presents the influence of aluminium mass concentration as well the cooling rate on the ultimate compressive strength. On the basis of the performed investigations it was found that the highest value of the ultimate compressive strength of 296.7 MPa has the MC MgAl6Zn1 alloy, and the lowest value of 245.9 MPa the MC MgAl3Zn1 alloy (both alloys cooled with a rate of 0.6°C/s). A change of the cooling rate of the analysed alloys causes an increase of the ultimate compressive strength. The highest increase of the R_c value in comparison to the cooling rate increase was found in case of the MC MgAl3Zn1 and MC MgAl9Zn1 alloy. An increase of the cooling rate up to the maximum value causes an increase of the ultimate compressive strength for the MCMgAl3Zn1 and MCMgAl9Zn1 alloy up to the value of 275.8 and 316 MPa adequately, as well is ca. 10-15 MPa higher in case of the MCMgAl6Zn1 and MCMgAl12Zn1 materials.

3.4. Database and the artificial neural network model

In this work two types of neural networks were used. First neural network were used to determine mechanical properties based on chemical composition and cooling rate. Model of neural network was used to verify correctness of experimental mechanical properties including Rockwell hardness in F scale, ultimate compressive strength (UCS, MPa) and metallographic characterisation (grain size, μm). The feed forward neural networks have been applied for calculations – Multi Layers were applied for calculations – Multi Layerceptron (MLP). The number of nodes in input was defined as eight, which correspond to cooling rate (0.6, 1.2 and 2.4°C/s) and alloy compositions, including the commonly used alloying elements in magnesium alloys, namely Al, Zn, Mn, Si, Cu, Fe and Mg. Number of nodes in output layer was defined as three – hardness, ultimate compressive strength and grain size (Fig. 27). One-of-N conversion type was applied for nominal variable, and minimax conversion for other variables. One-of-N conversion type using neurons number answering one nominal variable is an equal number of values achieved by this variable. In order to represent selected variable, appropriate neuron is activated and the rest of them stays inactive.
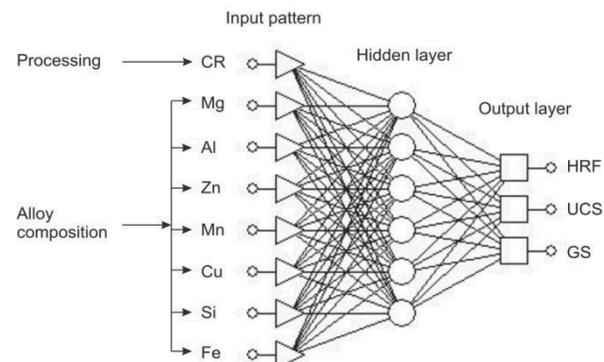

Fig. 27. Schematic diagram of the ANN model for prediction of properties of magnesium alloys

Data set was divided into three subsets: training, validating and testing ones. The result of design and optimisation process is network, which is characterized by an error of value, standard deviation and Pearson's correlation coefficient.

The number of hidden layers, number of nodes in these layers and the number of training epochs were determined by observing the neural forecast error for the training and validating sets. Neural network training was carried with errors back propagation method and conjugate gradient algorithm.

The neural network with one hidden layer and numbers of neurons in this layer as 6 was assumed to be optimal. The highest value of Pearson's correlation coefficient and the lowest value of standard deviation were achieved for MLP neural network that was trained by error back propagation method in 50 epochs and conjugate gradient algorithm in 59 epochs.

Table 16.
Quality assessment coefficients for applied neural networks for calculate of mechanical properties for testing set

Mechanical properties	Average of tested population	Absolute mean error	Standard error deviation	Standard deviation quotient	Pearson correlation coefficient
Hardness [HRF]	50.03	4.12	3.37	0.17	0.98
Ultimate compressive strength [MPa]	278.59	5.46	6.96	0.32	0.94
Grain size [μm]	118.36	6.43	7.59	1.85	0.91

The standard deviation ratio calculated for the training set is: 0.17 for hardness; 0.32 for ultimate compressive strength and 1.85 for grain size. Table 16 shows the values of errors, standard deviation ratios and Pearson correlation coefficients (R) for the calculated values of hardness ultimate compressive strength and grain size.
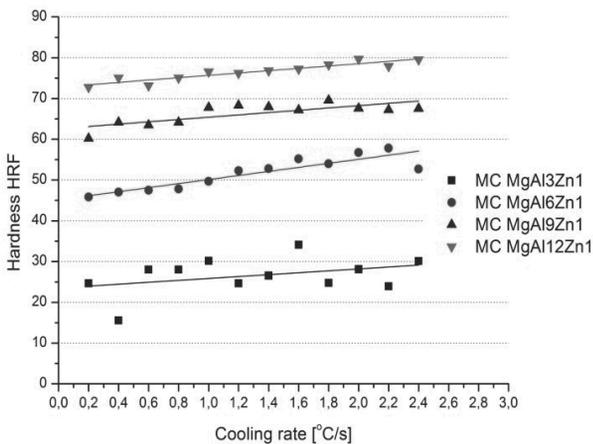

Fig. 28. Influence of cooling rate on the hardness of Mg-Al-Zn alloys

Mechanical properties of the magnesium alloys are strongly depended on cooling rate and aluminium content (Fig. 28), the hardness grows with increment of aluminium content and slightly with increment of cooling rate. In the opposite way it is with ultimate compressive strength. UCS grows with increment of cooling rate and slightly with increment of aluminium content (Fig. 29). Measuring errors occurred during testing did not exceed 5%.
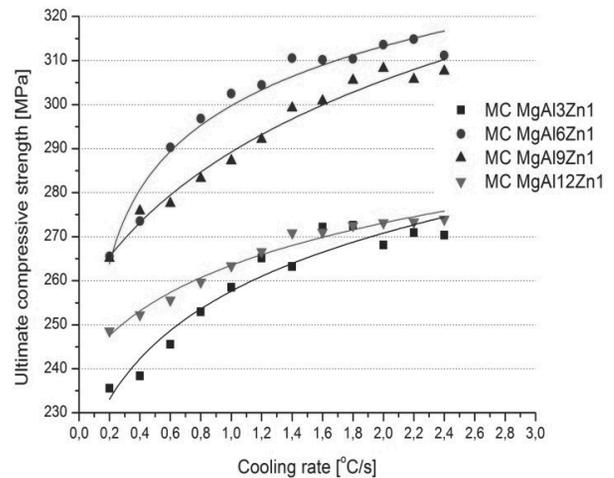

Fig. 29. The predicted influence of cooling rate on the ultimate compressive strength of Mg-Al-Zn alloys

On the basis of the worked out models of neural networks, the diagrams of the influence of the cooling rate and aluminium content were done on the hardness, ultimate compressive strength and grain size of the analyzed magnesium cast alloys (Figs. 30-32).
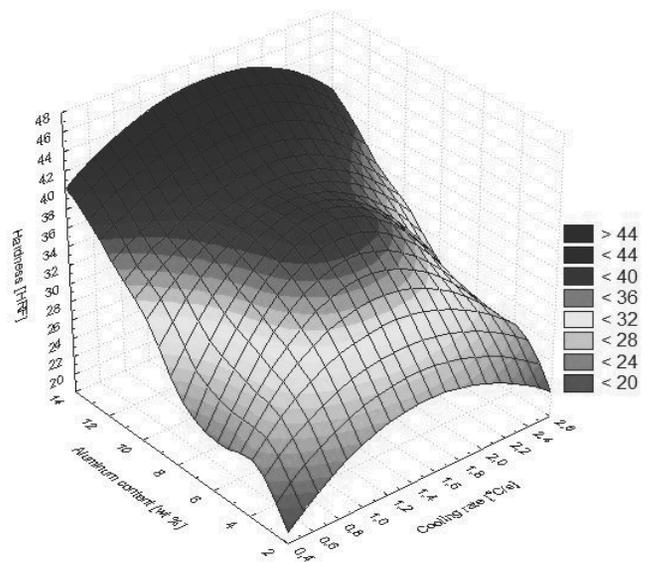

Fig. 30. Simulation of the cooling rate and aluminium content on hardness of the cast magnesium alloys
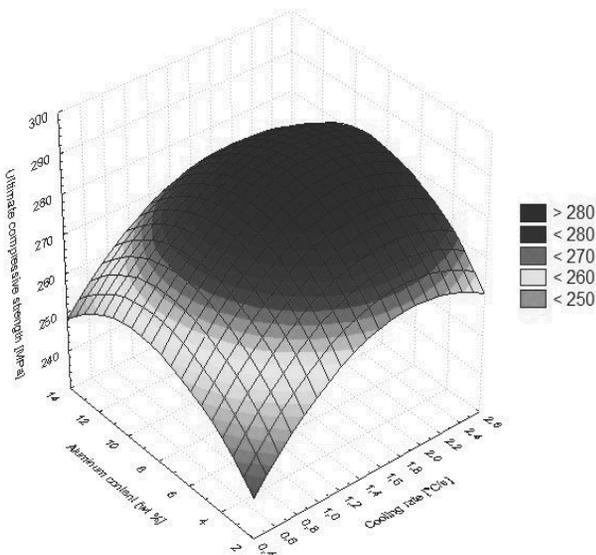
Fig. 31. Simulation of the cooling rate and aluminium content on ultimate compressive strength of the cast magnesium alloys
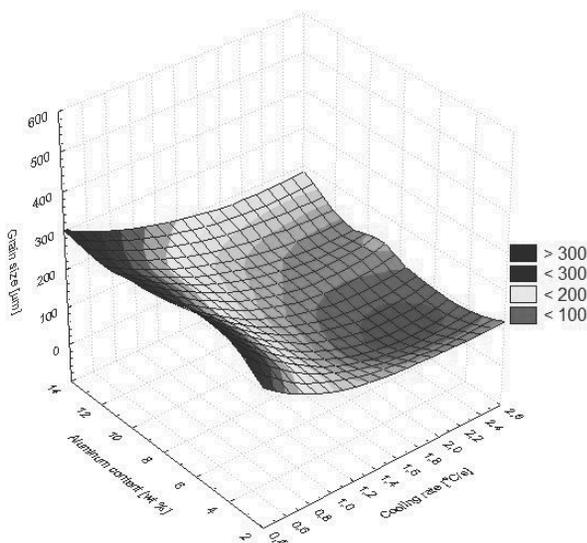

Fig. 32. Simulation of the cooling rate and aluminium content on grain size of the cast magnesium alloys

In second type of neural network data set was divided into three subsets: training, validating and testing ones. The data from the learning set has been used for the modification of the network weights, the data from the validating set, to evaluate the network during the learning process, while the remaining part of the values (the testing set) has been used for determining the network efficiency after ending completely the procedure of its creating.

The results used in the learning process and the network testing have been put to standardization. Scaling has been used in relation to the deviation from the minimal value, according to the mini-max function. The mini-max function transforms the variable domain to the range (0, 1). The type of the network,

the number of neurons in the hidden layer (layers), the method and learning parameters have been determined observing the influence of these quantities onto the assumed network quality coefficients.

The result of design and optimisation process is network, which is characterized by an error of value, standard deviation and Pearson's correlation coefficient. The quotient of standard deviations for errors and the data has been accepted, as the vital indicator of the model quality, made with the use of the neural network. The correctness of the network model may only be considered in case when the presented by networks forecasts are burdened with a smaller error than the simple estimation of the unknown output value.

Model of neural network was used to verify correctness of experimental crystallization temperatures including beginning of dendrite nucleation temperature T_{DN}, dendrite growth temperature T_G and solidus temperature T_{sol}. The feed forward neural networks have been applied for calculations – General Regression Neural Network (GRNN).
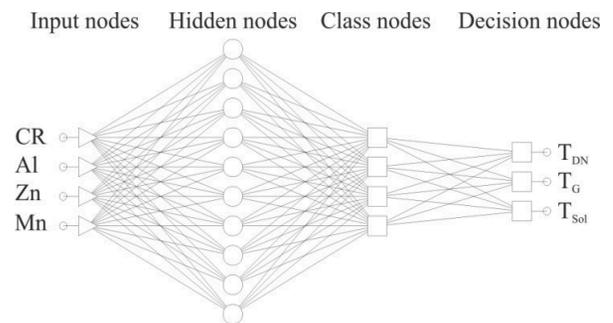

Fig. 33. Schematic diagram of the ANN model for prediction of properties of magnesium alloys

The number of nodes in input was defined as four, which correspond to cooling rate (0.6, 1.2 and 2.4°C/s) and alloy compositions, including the commonly used alloying elements in magnesium alloys, namely Al, Zn, Mn. Number of nodes in output layer was defined as three – dendrite nucleation temperature, dendrite growth temperature and solidus temperature (Fig. 33).

The number of hidden layers, number of nodes in these layers and the number of training epochs were determined by observing the neural forecast error for the training and validating sets. The neural network with two hidden layers and numbers of neurons in this layers as 10 and 4 were assumed to be optimal.

The standard deviation ratio calculated for the training set is: 0.16 for T_{DN}; 0.3 for T_G and 0.25 for T_{sol}. Table 17 shows the values of errors, standard deviation ratios and Pearson correlation coefficients (R) for the calculated values of crystallization temperatures.

On the basis of the worked out models of neural networks, the diagrams of the influence of the cooling rate and aluminium concentration, zinc and manganese concentration as well were done on the dendrite nucleation temperature, dendrite growth temperature and solidus temperature of the analyzed magnesium cast alloys (Figs. 34-39).

Table 17.
Quality assessment coefficients for applied neural networks for calculate of chemical composition and mechanical properties for testing set

Mechanical properties	Average of tested population	Absolute mean error	Standard error deviation	Standard deviation quotient	Pearson correlation coefficient
T_{DN} [°C]	613.01	3.52	3.97	0.16	0.98
T_G [°C]	605.77	5.29	7.69	0.3	0.97
T_{SOL} [°C]	451.38	7.86	11.34	0.25	0.98

The presented, on the MC MgAl12Zn1, MC MgAl9Zn, MC MgAl6Zn, MC MgAl3Zn alloy example results, confirm the correlation between the results of the laboratory research of Mg alloys with the results obtained out of the neural networks.
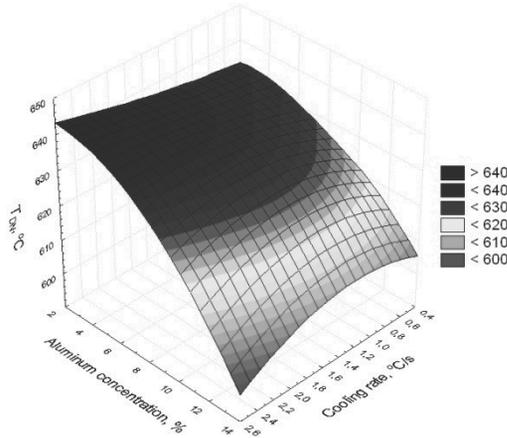

Fig. 34. Simulation of the cooling rate and aluminium concentration on beginnings of dendrite nucleation temperature
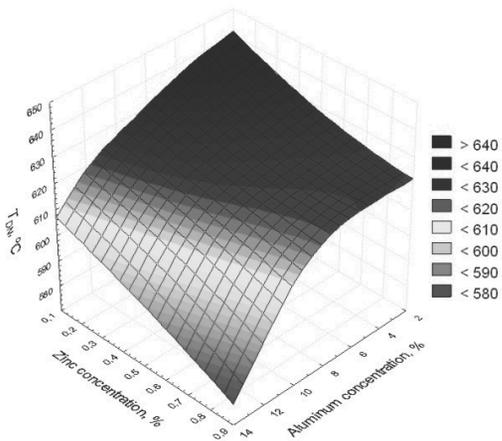

Fig. 35. Simulation of the aluminium and zinc concentration on beginnings of dendrite nucleation temperature
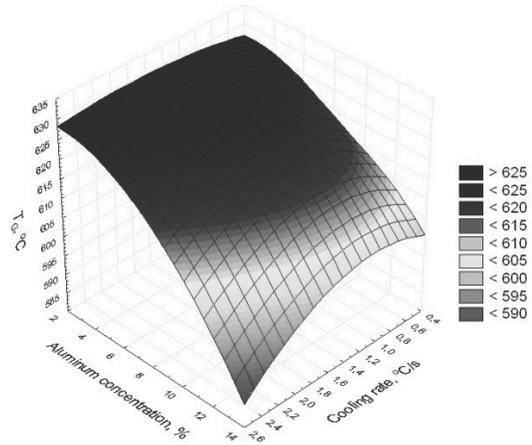

Fig. 36. Simulation of the cooling rate and aluminium concentration on dendrite growth temperature
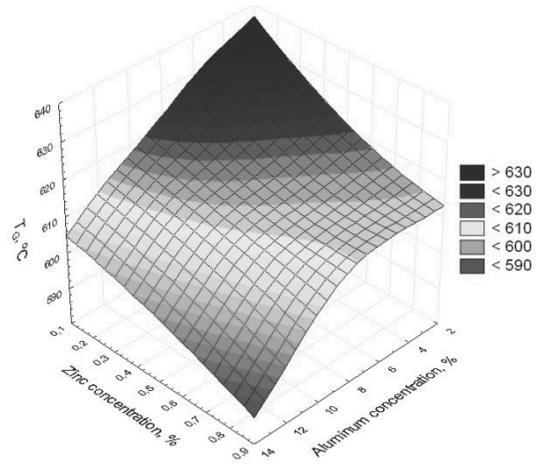

Fig. 37. Simulation of the aluminium and zinc concentration on dendrite growth temperature
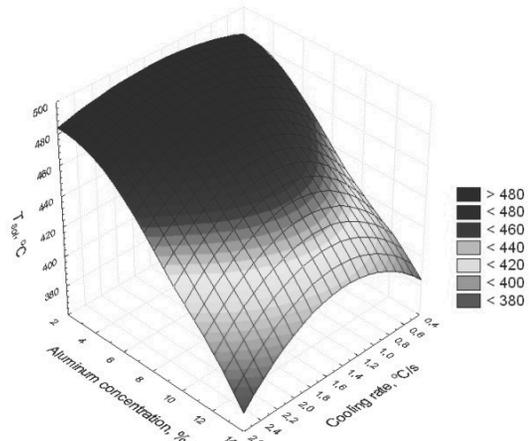

Fig. 38. Simulation of the cooling rate and aluminium concentration on solidus temperature
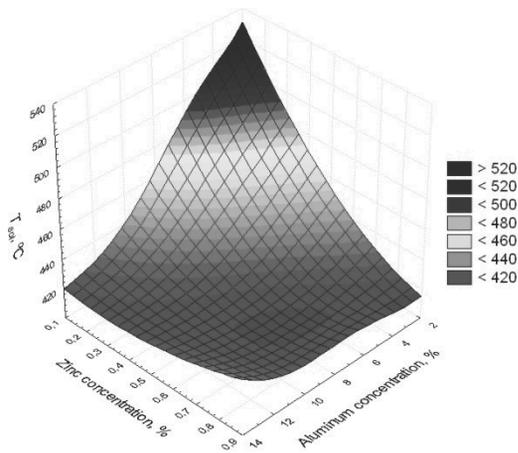
Fig. 39. Simulation of the aluminium and zinc concentration on solidus temperature

4. Conclusions

The new developed experimental cast magnesium alloys MC MgAl3Zn1, MC MgAl6Zn1, MC MgAl9Zn1, MC MgAl3Zn1 are characterising an α solid solution microstructure, which is the matrix, intermetallic $\gamma - Mg_{17}Al_{12}$ phase in a shape of plates, placed manly at grain border regions, needle shaped eutectic $(\alpha+\gamma)$ as well Mg_2Si containing precipitations characterized by edged outlines, also steroidal or needle shaped phases with high Mn and Al concentration are present (can be Al_8Mn_5 or $MnAl_4$). This research shows that the thermal analysis carried out on UMSA Technology Platform is an efficient tool for collecting and calculations of data about temperature and time of liquidus and solidus temperatures as well. Derivative thermo-analysis performed allowed to achieve several representative cooling, crystallization and calorimetric curves with characteristics points of crystallisation process for magnesium alloys. Description of characteristics points obtained from thermal-derivative analysis made it possible to get better understanding of the thermal processes occurred during crystallization kinetics of the investigated Mg alloys.

Solidification parameters are affected by the cooling rate. The formation temperatures of various thermal parameters are shifting with an increasing cooling rate. Increasing the cooling rate increases significantly the Mg nucleate temperature and decreases the solidus temperature simultaneously widens a solidification range. As expected, the results show that grain size reduces as the cooling rate increases. Increasing the cooling rate increases hardness and compressive ultimate strength of the examined magnesium alloys.

The artificial neural network model (ANN model) for predicting crystallization temperatures of crystallisable magnesium alloy was improved by refining pre-processing variables and using a more reasonable structure of hidden layers. The results show that the improved model could apparently decrease the prediction errors, and raise the accuracy of the prediction results. The improved ANN model was used to predict the crystallization temperatures of Mg-Al-Zn alloys. The predicted results were found to be in good agreement with the experimental data.

Acknowledgements

References

[1] P.J. Haines, Principles of thermal analysis and calorimetry, The Royal Society of Chemistry, Cambridge, UK, 2002.

[2] M.E. Brown, Introduction to thermal analysis. Techniques and application, Kluwer Academic Publisher, Netherlands, 2001.

[3] R.F. Speyer, Thermal analysis of materials, Marcel Dekker, 1994.

[4] P. Gabbott, Principles and applications of thermal analysis, Blackwell Publishing, UK, 2008.

[5] G.W.H. Hohne, W.F. Hemminger, H.J. Flammersheim, Differential Scanning Calorimetry, Springer-Verlag Berlin Heidelberg, 2003.

[6] P. Bassani, E. Gariboldi, A. Tuissi, Calorimetric analysis of AM60 magnesium alloy, Journal of Thermal Analysis and Calorimetry 80 (2005) 739-747.

[7] A. Saccone, D. Macciò, S. Delfino, F. H. Hayes, R. Ferro, Mg-Ce alloys, Experimental investigation by Smith thermal analysis, Journal of Thermal Analysis and Calorimetry 66 (2001) 47-57.

[8] B. Bronfin, N. Moscovitch, New magnesium alloys for transmission parts, Metal Science and Heat Treatment 48/11-12 (2006) 479-486.

[9] D. Eliezer, E. Aghion, F.H. Froes, Magnesium science and technology, Adv Mat Performance 5 (1998) 201-212.

[10] ASM Specialty Handbook-Magnesium and Magnesium Alloys, ed. M.M. Avedesian and H. Baker, ASM International, USA, 1999, 3-84.

[11] L.A. Dobrzański, T. Tański, L. Čížek, Influence of Al addition on structure of magnesium casting alloys, Journal of Achievements in Materials and Manufacturing Engineering 17 (2006) 221-224.

[12] I.J. Polmear, Light Alloys, London, 1995.

[13] K.U. Kainer, Magnesium – alloys and technologies, Wiley-VCH Verlag GmbH & Co. KG aA, Weinheim 2003, 33-341.

[14] L. Backuerud, G. Chai, J Tamminen, Solidification characteristics of aluminum alloys Vol.2 Foundry Alloys, AFS Skanaluminium, Stockholm, Sweden, 1990

[15] L. Backuerud, G. Chai, Solidification characteristics of aluminum alloys Vol. 3 Foundry Alloys, AFS Skanaluminium, Stockholm, Sweden, 1990.

[16] L.A. Dobrzański, R. Maniara, J. Sokołowski, W. Kasprzak , Effect of cooling rate on the solidification behavior of AC AlSi7Cu2 alloy, Journal of Materials Processing Technology 191 (2007) 317-320.

[17] L.A. Dobrzański, W. Borek, R. Maniara, Influence of the crystallization condition on Al–Si–Cu casting alloys structure, Journal of Achievements in Materials and Manufacturing Engineering 18 (2006) 211-214.

[18] S. Jura, Z. Jura, Theory ATD method in studies of Al alloys, Solidification of Metals and Alloys 28 (1996) 57-87 (in Polish).

[19] S. Jura, J. Sakwa, Application of thermal-derivative analysis to evaluate the mechanical properties of cast iron, Solidification of Metals and Alloys 5 (1982) 6-29 (in Polish).

[20] M. Malekan, S.G. Shabestari, Computer-aided cooling curve thermal analysis used to predict the quality of aluminum alloys, Journal of Thermal Analysis DOI 10.1007/s10973-010-1023-2.

[21] M. Kondracki, J. Gawroński, J. Szajnar, R. Grzelczak, K. Podsiadło, The study of the crystallization process MO95 brass based on ATD method, Archives of Foundry 2/4 (2002) 128-134 (in Polish).

[22] J. Gawroński, Crystallization of alloys, Thermal and derivation method (ATD), Archives of Foundry 16 (2005) 256-261 (in Polish).

[23] S. Jura, The essence of the ATD method. Modern methods for assessing the quality of alloys, PAN – Katowice, Institute of Foundry Silesian University, 1985 (in Polish).

[24] J. Adamiec, A. Kiełbus, J. Cwajna, The procedure of quantitative description of the structure of cast magnesium alloys, Archives of Foundry 6/18 (2006) 209-214 (in Polish).

[25] L.A. Dobrzański, T. Tański, Solid State Phenomena, Influence of aluminium content on behaviour of magnesium cast alloys in bentonite sand mould, Journal of Materials Processing Technology 147-149 (2009) 764-769.

[26] L.A. Dobrzański, T. Tański, L. Cížek, Heat treatment impact on the structure of die-cast magnesium alloys, Journal of Achievements in Materials and Manufacturing Engineering 20 (2007) 431-434.

[27] H. Baker, ASM Specialty Handbook. Magnesium and Magnesium Alloys, Avedesian (Ed.), ASM International, ISBN: 0871706571, (1999) USA.

[28] http://uwindsor.ca/umsa

[29] "Method and Apparatus for Universal Metallurgical Simulation and Analysis" – United States Patent, Patent No.: US 7,354,491 B2, Date of Patent: Apr. 8, 2008.

[30] Universal Metallurgical Simulator and Analyzer (UMSA) Platform for the Advanced Simulation of Melting and Solidification Processes, Software Information, 2002.

[31] E. Mares, J.H. Sokolowski, Artificial intelligence-based control system for the analysis of metal casting properties, Journal of Achievements in Materials and Manufacturing Engineering 40/2 (2010) 149-154.

[32] L.A. Dobrzanski, T. Tanski, J. Trzaska, L. Čížek, Modelling of hardness prediction of magnesium alloys using artificial neural networks applications, Journal of Achievements in Materials and Manufacturing Engineering 26/2 (2008) 187-190.

[33] L.A. Dobrzański, R. Honysz, Application of artificial neural networks in modelling of quenched and tempered structural steels mechanical properties, Journal of Achievements in Materials and Manufacturing Engineering 40/1 (2010) 50-57.

[34] T. Masters, Neural networks in practice, PWN, Warsaw, 1996 (in Polish).

[35] L.A. Dobrzański, S. Malara, J. Trzaska, Project of neural network for steel grade selection with the assumed CCT diagram, Journal of Achievements in Materials and Manufacturing Engineering 27/2 (2008) 155-158.

[36] W. Sitek, J. Trzaska, L.A. Dobrzanski, Evaluation of chemical composition effect on materials properties using AI methods, Journal of Achievements in Materials and Manufacturing Engineering 20 (2007) 379-382.

[37] J. Trzaska, L.A Dobrzański, A. Jagiełło, Computer programme for prediction steel parameters after heat treatment, Journal of Achievements in Materials and Manufacturing Engineering 24/2 (2007) 171-174.